https://doi.org/10.5194/essd-2024-516
Preprint. Discussion started: 29 January 2025

Open Access Earth System Science Data Discussions

Long history paddy rice mapping across Northeast China with deep learning and annual result enhancement method

Zihui Zhang[1,2], Lang Xia[1,2], Fen Zhao[1,2], Yue Gu[3], Jing Yang[1,2], Yan Zha[1,2], Shangrong Wu[1,2], Peng Yang[1,2]

[1]State Key Laboratory of Efficient Utilization of Arid and Semi-arid Arable Land in Northern China, the Institute of Agricultural Resources and Regional Planning, Chinese Academy of Agricultural Sciences, Beijing, 100081, China
[2]Institute of Agricultural Resources and Regional Planning, Chinese Academy of Agricultural Sciences/Key Laboratory of Agricultural Remote Sensing, Ministry of Agriculture and Rural Affairs, Beijing, 100081, China
[3]Department of Electrical and Computer Engineering, Rutgers University, New Brunswick, OK 08901, USA

Correspondence to: Lang Xia (xialang@caas.cn); Fen Zhao (zhaofen@caas.cn); Peng Yang (yangpeng@caas.cn)

Abstract Northeast China, a significant production base for paddy rice, has received lots of attention in crop mapping. However, understanding the spatiotemporal dynamics of paddy rice expansion in this region remains limited, making it difficult to track the changes in paddy rice planting over time. For the first time, this study utilized multi-sensor Landsat data and a deep learning model, the full resolution network (FR-Net), to explore the annual mapping of paddy rice for Northeast China from 1985 to 2023 (available at https://doi.org/10.6084/m9.figshare.27604839.v1, Zhang et al., 2024). First, a cross-sensor paddy training dataset comprising 155 Landsat images was created to map the paddy rice. Then, we developed the annual result enhancement (ARE) method, which considers the differences in category probability of FR-Net at different stages to diminish the impact of the limited training sample in large-scale and across-sensors paddy rice mapping. The accuracy of the paddy rice dataset was evaluated using 107954 ground truth samples. In comparison to traditional rice mapping methods, the results obtained using the ARE method showed a 6% increase in the F1 score. The overall mapping result obtained from the FR-Net model and ARE methods achieved high user accuracy (UA), producer accuracy (PA), F1 score, and Matthews correlation coefficient (MCC) values of 0.92, 0.95, 0.93, and 0.81, respectively. The study revealed that the area used for paddy rice cultivation in Northeast China increased from 1.11×10^4 km^2 to 6.45×10^4 km^2. Between 1985 and 2023, there was an overall expansion of 5.34×10^4 km^2 in the paddy rice cultivation area, with the highest growth (4.33×10^4 km^2) occurring in Heilongjiang province. This study shows that long-history crop mapping could be achieved with deep learning, and the result of paddy rice will be beneficial for making timely adjustments to cultivation patterns and ensuring food security.

1 Introduction

Paddy rice is an essential cereal crop globally and serves as the staple food for over half of the world's population (FAO, 2023). Therefore, it is crucial to gather accurate information on the temporal-spatial evolution characteristics and the long history of rice-growing districts. This knowledge can help us understand the intrinsic reasons affecting the temporal-spatial evolution in rice cultivation (You et al., 2021) and facilitate more efficient cultivation practices by adjusting the patterns of rice cultivation.

https://doi.org/10.5194/essd-2024-516
Preprint. Discussion started: 29 January 2025

Satellite remote sensing technology has been extensively utilized for mapping paddy rice on a regional or global scale, offering advantages over traditional ground-based monitoring methods (Yang et al., 2024). Based on the difference in spatial resolution, satellite data can be classified as low, medium, and high spatial resolution data. Low-resolution data, such as AVHRR and MODIS, provide long-history monitoring data but have limited spatial resolution and cannot recognize detailed spatial features (Xiao et al., 2005; Luo et al., 2020). High spatial resolution data, including GaoFen, QuickBird, IKONOS, etc., can recognize detailed spatial features on a meter scale. However, due to limited coverage availability and revisiting recycling, they are unsuitable for large-scale and long-history paddy rice monitoring. Medium-resolution data, such as Landsat, and Sentinel-2, can provide reasonable revisit recycling and sufficient spatial resolution in agriculture applications, making them widely used in crop mapping (Graesser and Ramankutty, 2017; Deines et al., 2019; Griffiths et al., 2020; Sun et al., 2021).

Commonly used paddy rice mapping methods can be categorized into phenology-based methods and data-driven algorithms. The phenology-based method involves using a spectral curve or index to illustrate the phenological differences between paddy rice and other crops (Ashourloo et al., 2022). While this method is simple and effective, it is challenged by cloud contamination, which leads to a lack of continuous data needed to observe phenotypic features (Dong et al., 2015). Therefore, the phenology-based method struggles to achieve precise long-history mapping across large areas. Data-driven algorithms include traditional machine learning and deep learning methods. Traditional machine-learning algorithms usually rely on manual feature extraction, which may be less effective in feature abstraction (Goldberg et al., 2021; Khojastehnazhand and Roostaei, 2022). Particularly in complex cropping systems, traditional machine-learning algorithms may fail to differentiate between paddy rice and other crops (Zhong et al., 2019; Kamir et al., 2020; Gao et al., 2023).

The demand for accurate and efficient crop mapping is increasing as computer technology advances rapidly. Deep learning models such as RNN (Recurrent Neural Network) (Thorp and Drajat, 2021) and semantic segmentation networks (Yang et al., 2022) are increasingly being used for crop identification (Akkem et al., 2023). RNN can remember and recurse, allowing it to capture the context in sequential data, thus abstracting the feature information of temporal remote sensing images and performing crop mapping (Kong et al., 2019). However, RNN requires continuous clear-sky satellite images as input, which is difficult to obtain due to cloud contamination. Under a cloud scene, the sequence feature learned by the model is different from the test dataset, leading to decreased performance in crop mapping (Chen et al., 2021; Akkem et al., 2023). Semantic segmentation is a computer vision task that aims to assign category labels to individual pixels in an image, achieving pixel-level classification (Lu et al., 2023; Sun et al., 2023). Compared with the RNN, the semantic segmentation model can automatically learn spectral and spatial features from one or more satellite images for end-to-end classification, without relying on the sequence feature behind the time-series data. Therefore, the input data of the semantic segmentation model is more flexible (Gao et al., 2023; Lu et al., 2023), making it more suitable for large-scale crop mapping with a long history (Yang et al., 2022).

The semantic segmentation model offers advantages for large-scale mapping. However, determining the final mapping result from multiple annual results remains a challenge for large-scale paddy rice mapping (Feng et al., 2023). Paddy rice exhibits distinct spectral and spatial characteristics at different growth stages, making it difficult to obtain enough training samples to

https://doi.org/10.5194/essd-2024-516
Preprint. Discussion started: 29 January 2025

cover the full range of phenology on a large scale. In this situation, the trained model may fail to learn the features presented in the test dataset on a large scale, and the results generated by the semantic segmentation model under different phenology in one year may present different accuracies (Zhang et al., 2014; Xia et al., 2022). In practice, the commonly used method to obtain yearly final results is to average or overlay the different paddy rice results within the year (Feng et al., 2023). Unfortunately, this approach simply merges paddy rice results in different phenology and does not consider the most accurate paddy rice results in different phenology. As a result, the final annual paddy rice result would inherit the errors from the paddy rice results in different phenology.

The significant increase in rice cultivation in Northeast China has caught the attention of researchers who are interested in understanding the spatial and temporal distribution of rice in the region. The area used for growing paddy rice has expanded by 144 % from 2000 to 2017 (Xin et al., 2020), and the northern boundary of paddy rice cultivation has shifted about 25 km northward from 1984 to 2013 (Liang et al., 2021). Despite various efforts to map paddy rice cultivation (Table 1), there is still a lack of detailed spatial data for the entire Northeast China. This data gap is hindering the accurate assessment of crop methane emissions and the development of sustainable agricultural policies.

Table 1 Relevant mapping datasets of paddy rice in China

Coverage of Northeast China	Time range/Span	Data source	Spatial resolution	Reference
Partly	1990–2020/5years	Landsat	30 m	(Zhang et al., 2023)
Partly	2015/yearly	Sentinel-1	10 m	(Onojeghuo et al., 2018)
Partly	2020/yearly	MODIS	500 m	(Shao et al., 2023)
Partly	2020/yearly	GF-6 WFV	16 m	(Guo and Ren, 2023)
Partly	2013–2021/yearly	Landsat	30 m	(Xuan et al., 2023)
Fully	2000–2017/yearly	MODIS	500 m	(Xin et al., 2020)
Fully	2017–2019/yearly	Sentinel-2	10 m	(Ni et al., 2021)
Fully	2017–2022/yearly	Landsat	30 m	(Shen et al., 2023)

In this study, we focused on paddy rice in Northeast China and used long-term Landsat data from different sensors to track the annual changes in paddy rice fields for the first time. The contribution of this study is (1) constructing a cross-sensor training dataset for paddy rice using Landsat 5 TM and Landsat 8 OLI sensors, (2) proposing an annual results enhancement (ARE) method based on category probability to improve annual mapping result of paddy rice under different phenology within a year, and (3) generating yearly paddy rice maps with 30m spatial resolution in Northeast China from 1985 to 2023 for the first time. These consistent paddy rice maps can be utilized for monitoring paddy rice dynamics and assessing the effects of land-use policies.

https://doi.org/10.5194/essd-2024-516
Preprint. Discussion started: 29 January 2025

2 Materials and Methods

2.1 Study area

The study area (38°43′8.4″-53°33′50.4″N, 111°8′38.4″-135°5′45.6″E) shown in Fig.1(a) is located in Northeast China, which includes Heilongjiang province, Jilin province, Liaoning province, and northeastern Inner Mongolia. It covers approximately 1.26×10^6 km^2, accounting for 13.13% of China's total area (Zhang et al., 2014; Xin et al., 2020). Northeast China experiences a frigid zone with a continental monsoon climate and an average elevation of 450 m. The average annual temperature is about 4.37°C, and the average annual precipitation is about 800 mm. One crop per year is cultivated in this region under these hydrothermal conditions (Xin et al., 2020). The primary crops are rice (Zheng et al., 2023), maize (Shi et al., 2022), and soybeans (Huang et al., 2022), each with distinct growth periods. Paddy rice production in Northeast China consistently accounts for over 20% of the total paddy rice production in China. The cultivation patterns of paddy rice have undergone significant transformations, becoming a prominent driver of land use change in the study area (Griffiths et al., 2019; Jin and Zhong, 2022).

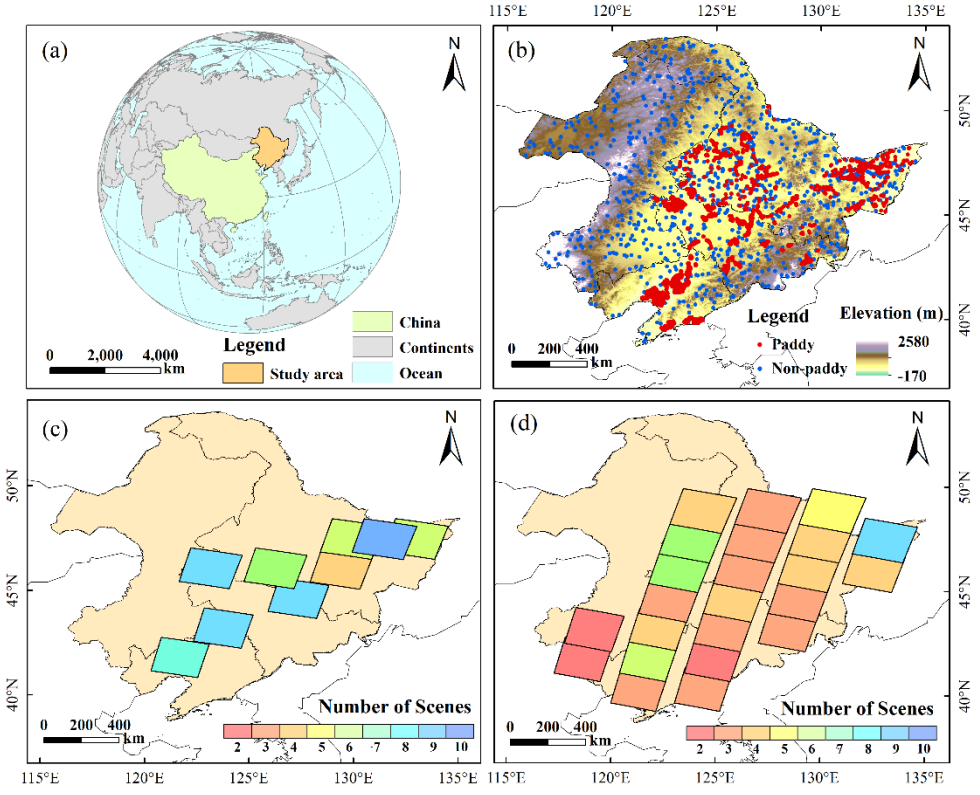

Figure 1: (a) Location of the study area. (b) Distribution of ground truth data in Northeast China. (c), (d) are the number of training datasets for Landsat 5 and Landsat 8/9, respectively.

https://doi.org/10.5194/essd-2024-516
Preprint. Discussion started: 29 January 2025

2.2 Methods

2.2.1 FR-Net

A Full-Resolution network (FR-Net) was proposed to tackle the problem of low accuracy in edge segmentation caused by the loss of spatial information in deep semantic segmentation networks. The core component of FR-Net, aimed at achieving high-resolution semantic segmentation and producing high-precision segmentation outputs, is the multi-resolution feature fusion unit (MRFU). The MRFU comprises 3×3 convolutional layers with a stride of 1, a batch normalization (BN) layer, and a rectified linear unit (ReLU) activation layer. These components work together to control and fuse feature streams with different resolutions. For the specific structure and implementation of FR-Net and MRFU, please refer to the published article by Xia et al. (2022). FR-Net has a simple structure and requires minimal computational resources, making it suitable for extracting characteristic information from Landsat data and mitigating the issue of gradient disappearance.

2.2.2 Annual results enhancement method

The commonly used method (Graesser and Ramankutty, 2017) to obtain the final mapping results from multiple mapping results within a year in the current large-scale semantic segmentation model for single paddy rice calculated following Eq.(1):

$$Result = \begin{cases} nonpaddy. else \\ paddy, \forall i \in [1, \dots m]: Result_i = paddy \end{cases}, \quad (1)$$

where $Result_{pre}$ is the final annual mapping results, m means the number of images during the paddy rice phenological period within the year, i refer to order number of images, $Result_i$ is the result from the deep learning model, which includes two categories: paddy and non-paddy. Eq.(1) states that the output results of the deep learning model indicate that if there is a mapping result for any paddy period, the result for that specific year is classified as paddy; otherwise, it is classified as non-paddy.

In large-scale paddy rice mapping, there are noticeable differences in the spectral and texture characteristics of the rice at different growth stages throughout the year (Yin et al., 2020; Pan et al., 2021). Furthermore, the high cost of generating high-quality training samples presents a significant challenge in ensuring comprehensive coverage of diverse phenological periods (Yeom et al., 2021). Therefore, errors may vary in paddy rice results for different phenological periods within the year. Simply employing equation (1) would overlook this, perpetuate errors in different phenological periods, and reduce the accuracy of the final paddy rice map. To enhance the accuracy of annual maps, we proposed the annual results enhancement (ARE) method based on a comprehensive consideration of paddy rice mapping category probability at different phenological periods. This method differs from previous studies, as demonstrated in Eq.(2):

$$t = Arg\big(max(|P_i - 0.5|)\big), i, t \in [1, \dots, m]$$

$$Result = \begin{cases} nonpaddy, P_t < 0.5 \\ paddy, P_t > 0.5 \end{cases}, \quad (2)$$

https://doi.org/10.5194/essd-2024-516
Preprint. Discussion started: 29 January 2025

where *i* refers to the order number of images within the growth period, P_i is the category probability output by FR-Net for images *i*, *max*() means to obtain the maximum, *Arg*() means to get the order number of images, *t* represents the image corresponding to the highest P_i among *m* images, P_t is the category probability output by FR-Net for images *t*, *Result* is the final paddy rice map within the year.

The ARE method considers the difference in category probability when mapping results show different phenology. It identifies the most accurate annual paddy rice mapping result by choosing the highest category probability among different mapping results. This approach can reduce the impact of feature differences between training and test data sets caused by limited training samples on large-scale mapping. It also enhances the annual paddy rice mapping accuracy of the semantic segmentation model.

2.3 Dataset and processing

2.3.1 Landsat TM and OLI images

A total of 13809 Landsat Collection 2 Level-2 surface reflectance products with a spatial resolution of 30 m were downloaded during the paddy rice growth periods of 1985-2023 for generating paddy rice maps (Fig.2). These images included Landsat 5 Thematic Mapper (TM) data from 1985 to 2011, as well as Landsat 8/9 Operational Land Imager (OLI) data from 2013 to 2023. Landsat 7 was adversely affected by stripes, resulting in poor data quality, hence the lack of 2012 imagery acquisition, processing, and analysis. In addition, we selected the b2, b3, b4, b5, b6, b7 bands of Landsat 8/9 OLI and b1, b2, b3, b4, b5, b7 bands of Landsat 5 TM images to map the paddy rice.

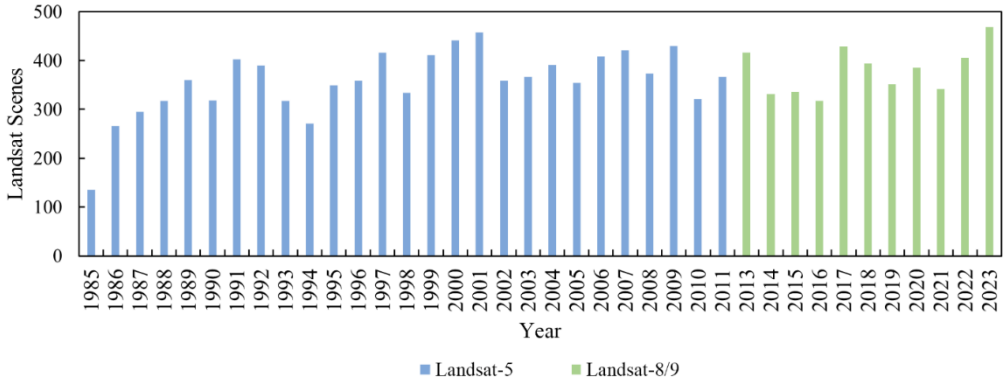

Figure 2: Number of Landsat images from 1985 to 2023 used in this study.

2.3.2 Ground truth dataset

The ground truth dataset was collected from field surveys and Google Earth conducted across Northeast China. Before 2002, very high resolution (VHR) was unavailable, so the VHR data was obtained from Google Earth spanning from 2002 to 2023. The field survey data was gathered from 2011 to 2023. Paddy data from the field survey were identified using a digital camera and a Global Positioning System (GPS) receiver (Garmin GPSMAP 78s) with an accuracy of ±3 m (Xia et al., 2022). The

https://doi.org/10.5194/essd-2024-516
Preprint. Discussion started: 29 January 2025

ground truth dataset comprises 68856 samples of paddy and 39098 samples of non-paddy (Fig.1(b)). More specifically, 21254 samples of paddy and 13160 samples of non-paddy were obtained from the field survey, while 47602 samples of paddy and 25938 samples of non-paddy were obtained from Google Earth VHR data. This dataset was used to evaluate the accuracy and reliability of the paddy rice mapping results.

2.3.3 Construction of training and test dataset

The training and test data were obtained from the paddy mapping results based on eXtreme Gradient Boosting (XGBoost) maps after manual correction, as described below. First, we identified paddy and non-paddy regions of interest (ROIs) in Landsat images, and used these ROIs to train the XGBoost model. The XGBoost model was then utilized to initially obtain the temporal spatial distribution of paddy rice in the selected images. After that, manual correction was conducted to correct the temporal results of XGBoost. This process resulted in a high-precision paddy rice mapping dataset that covers the years from 1985 to 2023 with a total of 155 scenes (Fig.1(c), (d)). This dataset is divided into 3:1 for training and validation (Supplementary Table 1).

We have generated the training and validation labels for the FR-Net as below (available at https://doi.org/10.6084/m9.figshare.28283606, Zhang, 2025). Both the Landsat images and their corresponding masks were rotated by 5°. Subsequently, all the Landsat images and masks were cropped into several small images with dimensions of 256 × 256. These small images covered the Landsat images completely without any overlap, and any cropped image without paddy rice pixels was removed. The training and validation sets for Landsat 5 images were 29906 and 9968, respectively, the training and validation sets for Landsat 8/9 images were 50956 and 16985, respectively.

2.4 Agricultural statistical data during 1985-2022

We have utilized agricultural statistical data obtained from district, municipal, and provincial statistical bureaus dating from 1985 to 2022. The statistical data we used includes paddy planted areas, which helped us confirm the accuracy and reliability of the paddy rice maps we provided for Northeast China. This confirmation was based on the total area under cultivation per year and temporal variations. As agricultural statistical data for 2023 are not yet available, we validated the paddy rice maps from 1985 to 2022. The accuracy of the paddy rice map in 2023 was verified using the ground truth data obtained in 2023.

2.5 Model training and accuracy assessment

The model was implemented on a workstation equipped with a single NVIDIA GeForce RTX 3090 GPU, Intel i5-13400K CPU, and 1 TB SSD. We installed Keras 2.5, Tensorflow 2.6, CUDA 11.3, and cuDNN 8.2 on the workstation for model training. The Adam with a constant learning rate of 0.001 was selected as the optimizer, and the batch size was 8. The model was trained five times, and the one with the best validation accuracy was used for mapping the paddy rice.

In this study, we used the user accuracy (UA), producer accuracy (PA), F1 score, and Matthews correlation coefficient (MCC) to evaluate the accuracy of the long history paddy rice maps, as shown in Eq.(3)–(6):

https://doi.org/10.5194/essd-2024-516
Preprint. Discussion started: 29 January 2025

$$UA = \frac{TP}{TP+FP}, \quad (3)$$

$$PA = \frac{TP}{TP+FN}, \quad (4)$$

$$F1 = 2 \times \frac{UA*PA}{UA+PA}, \quad (5)$$

$$MCC = \frac{TP \times TN - FP \times FN}{\sqrt{(TP+FP)(TP+FN)(TN+FP)(TN+FN)}}, \quad (6)$$

where TP is the true positive, TN is the true negative, FP is the false positive, and FN is the false negative. UA, PA, and F1 score are commonly used metrics in the evaluation of classification accuracy (Foody, 2020; Xu et al., 2023), and F1 is a harmonic mean of precision and recall. The MCC is a comprehensive performance indicator that takes into account TP, TN, FP, and FN to reduce the randomness and imbalance of classification results (Zhu, 2020).

3 Results

3.1 Performance of ARE method

To verify the necessity of using the ARE method to enhance the results of paddy rice mapping, we conducted a comparison between the results obtained using ARE and those obtained from overlay or single temporal methods (Fig.3). Our findings indicate that there are significant variations in the results for paddy rice with different phenologies. The single and overlay methods have limitations, while the ARE method can effectively address these limitations by considering the differences in category probability mapping results at different phenological stages. This enhances the accuracy and reliability of paddy rice maps. In addition, the presence of salt and pepper noise in images can significantly impact the accuracy of plot segmentation. However, the ARE method can produce clearer plot edges and demonstrate improved classification performance compared to the results of the paddy rice maps that were overlayed at different periods.

https://doi.org/10.5194/essd-2024-516
Preprint. Discussion started: 29 January 2025

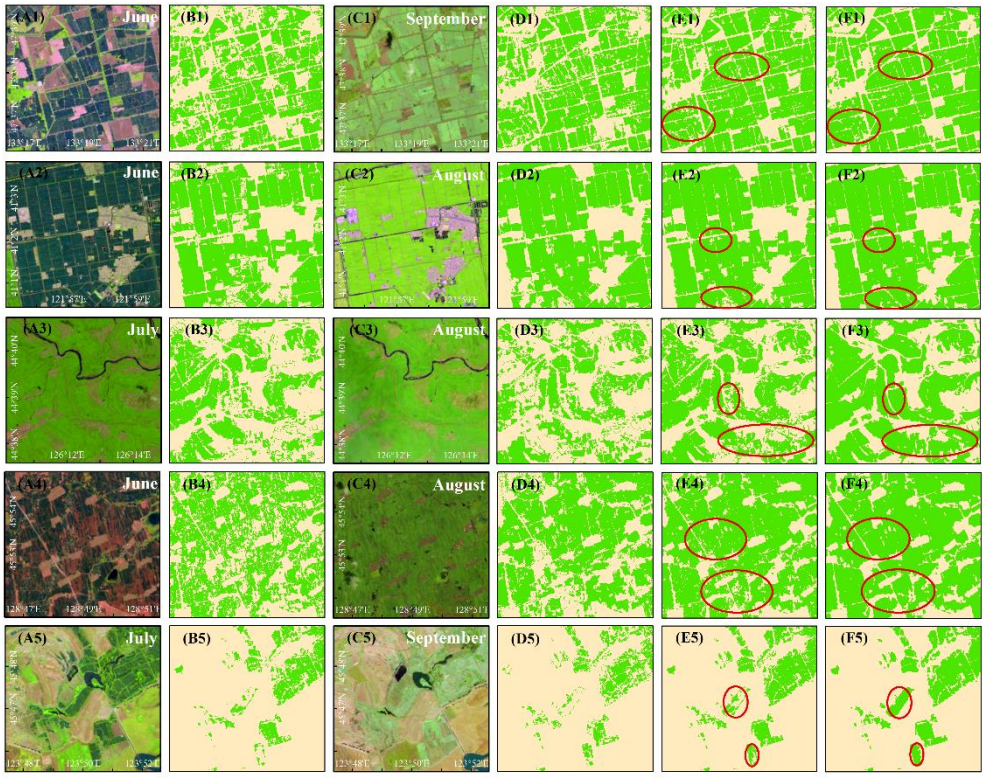

Figure 3: Comparison of paddy rice maps between ARE, single temporal, and overlay methods using Landsat 5 TM and Landsat 8 OLI images. (A1)-(A3), (C1)-(C3) represent pseudo-colored maps of three regions in the Landsat 8 images (bands 6, 5, and 4) from June to September. (A4), (A5), (C4), and (C5) represent pseudo-colored maps of two regions in the Landsat 5 images (bands 5, 4, 3) from June to September. (B1)-(B5) display the paddy rice maps corresponding to the images in (A1)-(A5). (D1)-(D5) shows the paddy rice maps corresponding to the images in (C1-(C5). (E1)-(E5) are the overlay results of the paddy rice maps from June to September. (F1)-(F5) depict ARE paddy rice maps. The red circles in the overlay and ARE maps indicate areas with significant differences in paddy rice.

We chose areas in Northeast China that were captured by multiple Landsat scenes at different growth stages. We also had corresponding ground truth data to quantitatively evaluate the performance of the ARE method. We used a confusion matrix to compare and analyze the performance of the ARE method (Table 2). In comparison to traditional rice mapping methods, the results obtained using the ARE method showed a 6% increase in the F1 score. The F1 score of the ARE results was 0.93, which is higher than the F1 score of 0.87 for the overlay results. These results indicate that the ARE method exhibits higher accuracy and better performance, while the overlay maps and single temporal results demonstrated more severe misclassification and omission.

Table 2 Confusion matrix for ARE results, overlay results, and single temporal results based on ground truth data.

Truth / Prediction		Result 1		Result 2		Overlay maps		ARE maps	
		Paddy	Non-paddy	Paddy	Non-paddy	Paddy	Non-paddy	Paddy	Non-paddy
Field	Paddy	6306	1453	6638	1273	7334	945	7716	541

https://doi.org/10.5194/essd-2024-516
Preprint. Discussion started: 29 January 2025

survey	Non-paddy	2196	3811	1864	3991	1168	4319	786	4723
	Total	8502	5264	8502	5264	8502	5264	8502	5264
	F1 score	0.78		0.81		0.87		0.92	
VHR	Paddy	13594	2700	14529	2157	15812	1454	17266	893
	Non-paddy	5446	7675	4511	8218	3228	8921	1774	9482
	Total	19040	10375	19040	10375	19040	10375	19040	10375
	F1 score	0.77		0.81		0.87		0.93	
All	Paddy	19900	4153	21167	3430	23146	2399	24982	1434
	Non-paddy	7642	11486	6375	12209	4396	13240	2560	14205
	Total	27542	15639	27542	15639	27542	15639	27542	15639
	F1 score	0.77		0.81		0.87		0.93	

3.2 Performance of the paddy rice results

3.2.1 Accuracy evaluation

The performance of the FR-Net and ARE methods for paddy rice mapping was evaluated using confusion matrices and metrics such as UA, PA, F1, and MCC based on ground truth data (Table 3). The annual confusion matrix metrics were all found to be at least 0.90 for UA, 0.89 for PA, 0.90 for F1, and 0.77 for MCC. The overall confusion matrices for UA, PA, F1, and MCC are 0.92, 0.95, 0.93, and 0.81, respectively. These findings demonstrate the effectiveness of the FR-Net and ARE methods in accurately mapping long-history paddy rice cultivation in Northeast China, confirming their strong generalization across both time and space.

Table 3 Confusion matrix of paddy rice maps.

Year	Validation	Truth		UA	PA	F1	MCC
		Paddy	Non-paddy				
2002	Paddy	1649	32	0.91	0.98	0.95	0.77
	Non-paddy	156	498				
2003	Paddy	2364	103	0.92	0.96	0.94	0.81
	Non-paddy	197	1182				
2004	Paddy	854	109	0.93	0.89	0.91	0.86
	Non-paddy	62	1061				
2005	Paddy	793	98	0.91	0.89	0.90	0.82
	Non-paddy	76	834				
2006	Paddy	917	94	0.92	0.91	0.91	0.84
	Non-paddy	78	962				
2007	Paddy	1096	75	0.92	0.94	0.93	0.83
	Non-paddy	97	847				
2008	Paddy	1872	135	0.91	0.93	0.92	0.81
	Non-paddy	176	1274				
2009	Paddy	1539	149	0.90	0.91	0.91	0.81
	Non-paddy	163	1472				
2010	Paddy	1672	168	0.91	0.91	0.91	0.81
	Non-paddy	173	1527				
2011	Paddy	1937	175	0.90	0.92	0.91	0.81
	Non-paddy	206	1864				
2013	Paddy	2176	168	0.92	0.93	0.92	0.82
	Non-paddy	193	1647				

https://doi.org/10.5194/essd-2024-516
Preprint. Discussion started: 29 January 2025

2014	Paddy	3079	195	0.91	0.94	0.93	0.80
	Non-paddy	287	1764				
2015	Paddy	3346	157	0.92	0.96	0.94	0.82
	Non-paddy	275	1762				
2016	Paddy	3869	273	0.91	0.93	0.92	0.80
	Non-paddy	373	2618				
2017	Paddy	5746	247	0.92	0.96	0.94	0.79
	Non-paddy	493	2372				
2018	Paddy	4923	213	0.92	0.96	0.94	0.80
	Non-paddy	446	2474				
2019	Paddy	5239	224	0.91	0.96	0.93	0.79
	Non-paddy	508	2405				
2020	Paddy	4837	162	0.91	0.97	0.94	0.77
	Non-paddy	473	1772				
2021	Paddy	5368	235	0.92	0.96	0.94	0.79
	Non-paddy	437	2137				
2022	Paddy	5219	259	0.94	0.95	0.94	0.83
	Non-paddy	358	2473				
2023	Paddy	4783	238	0.93	0.95	0.94	0.83
	Non-paddy	351	2644				
Overall	Paddy	63278	3509	0.92	0.95	0.93	0.81
	Non-paddy	5578	35589				

3.2.2 Compare with agricultural statistics

The accuracy of the paddy rice maps we provided has been confirmed using agricultural statistics data. These maps have demonstrated strong consistency and correlation with the agricultural statistics data, as shown in Fig.4 (a). The high R^2 value of 0.93 indicates a robust positive correlation between the provided paddy rice maps and the agricultural statistics data. However, the paddy rice cultivation areas were overestimated, as shown in Fig.4 (b). This suggests that while these maps provide relatively accurate information on the distribution of paddy cultivation, they cannot be completely accurate. It is essential to consider potential sources of error or uncertainty in both the agricultural statistics data and the mapping methodology, including factors such as data collection methods, spatial resolution, and limitations of the statistical models used. Despite these potential limitations, Figure 4 provides strong evidence supporting the credibility of the provided paddy rice maps.

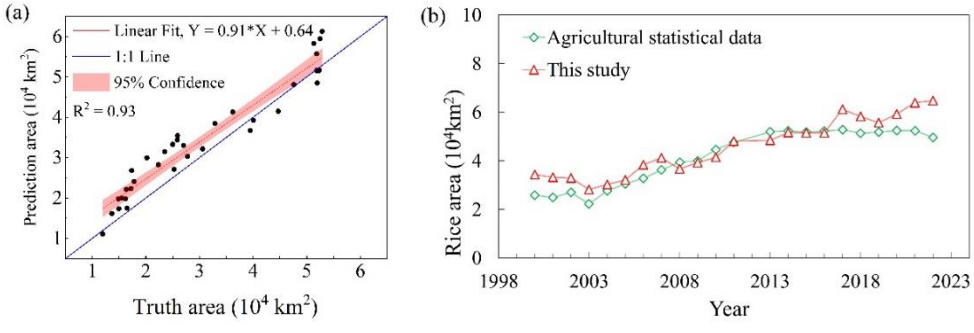

Figure 4 Comparison of paddy rice maps with agricultural statistical data.

https://doi.org/10.5194/essd-2024-516
Preprint. Discussion started: 29 January 2025

Open Access Earth System Science Data Discussions

240 **3.2.3 Comparison with other paddy rice datasets**

In this study, we compared the paddy rice products with other representative products (Fig.5). These included products generated by the coarse resolution of MODIS data (Liu et al., 2018), the phenology-based method using optical Landsat data (Zhang et al., 2023), and the combined use of Sentinel-1/2 SAR and optical data (Shen et al., 2023). The results showed that the paddy rice products obtained from MODIS data overestimation due to fragmented plots and mixed pixels in rice cultivation
245 areas, as shown in Fig.5 (C1)-(C4). Similarly, the paddy rice products generated using the phenology-based method with optical Landsat data demonstrated omissions, as illustrated in Fig.5 (D1)-(D4). In contrast, the results of this study, shown in Fig.5 (B1)-(B4), reveal that most paddy pixels were well recognized using the FR-Net and ARE methods. Furthermore, the mapping results that combined SAR and optical data also exhibited some leakage of the paddy pixels. The speckle noise from Sentinel-1 contributed to an increase in salt-and-pepper noise in the paddy rice results, which in turn reduced the mapping
250 accuracy, as illustrated in Fig.5 (E1)-(E4). The deep network FR Net and ARE achieved a more complete representation of rice plots with clearer boundaries and improved mapping accuracy compared to individual phenological methods.

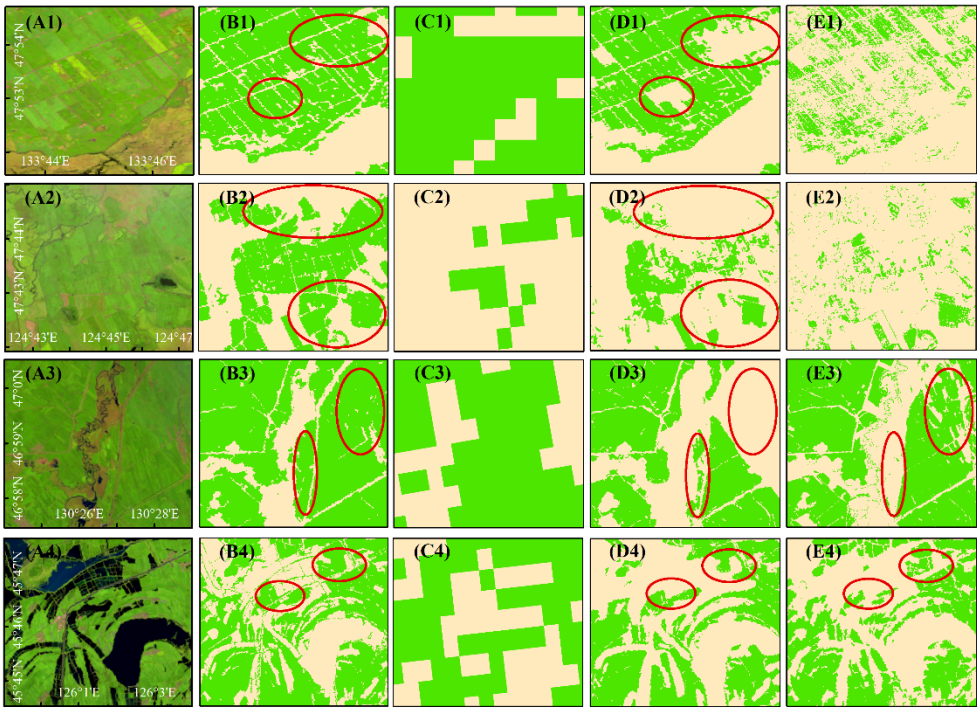

Figure 5: Comparison of the paddy rice products of this study with the existing products. (A1)-(A4), represents pseudo-colored (bands 6, 5, and 4) of Landsat 8/9 images. (B1)-(B4) is the result of this study. (C1)-(C4) shows the paddy rice with MODIS data.
255 **(D1)-(D4) demonstrate the paddy rice with Landsat data. (E1)-(E4) depict the paddy rice maps using Sentinel-1 and Sentinel-2 images. The red circles indicate areas with significant differences in paddy rice.**

https://doi.org/10.5194/essd-2024-516
Preprint. Discussion started: 29 January 2025

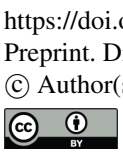

Open Access Earth System Science Data Discussions

3.3 Spatiotemporal patterns of paddy rice from 1985 to 2023

In the long history of paddy rice mapping, clouds have posed a challenge that hinders the accuracy of the annual mapping results. In certain areas, it is difficult to obtain clear-sky observation data during the growth period of paddy rice, resulting in limited coverage in the annual mapping results. Figure 6 shows the study area, which lacks at least one clear-sky observation during the yearly growth stage of paddy rice. This figure demonstrates that in Northeast China, there are areas where at least one clear-sky observation during the annual growth stage of paddy fields is not possible. To improve the quality of the yearly mapping results in this study, the missing pixels were filled based on good observations from before and after the year, and year-to-year cloud coverage maps were obtained.

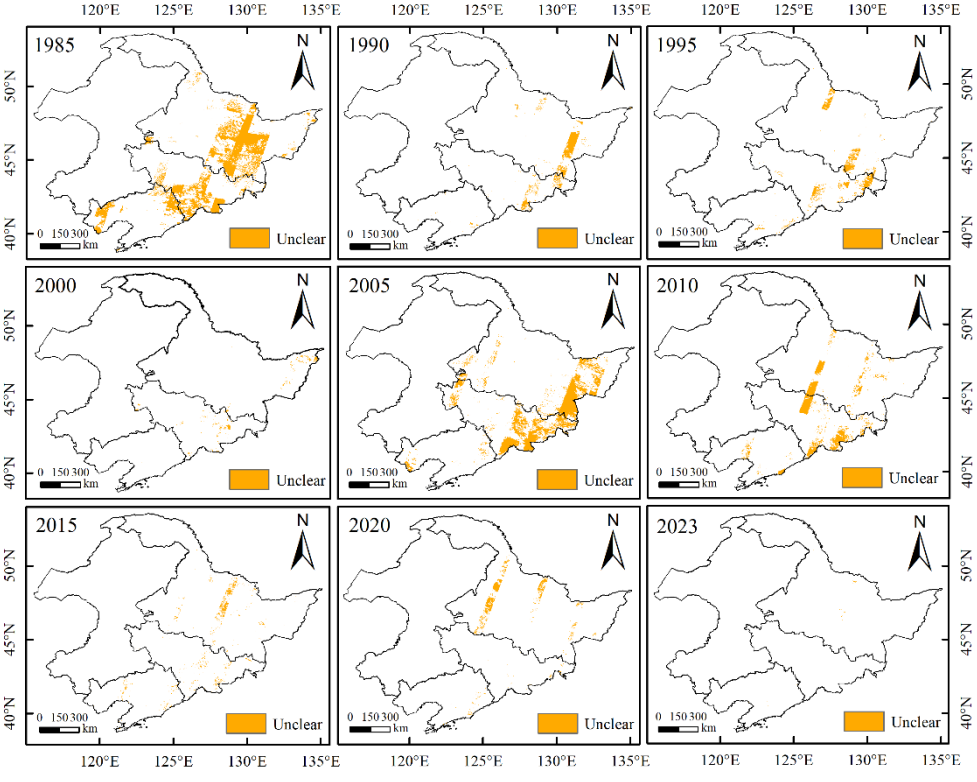

Figure 6: Areas lack at least one clean-sky observation during the annual growth stage of paddy.

Figure 7 shows the filled paddy cultivation in Northeast China from 1985 to 2023, mainly distributed along river banks. A noteworthy increase in the area of paddy rice cultivation was observed in the central region of the study area between 1985 and 1990. Additionally, there was a significant expansion of paddy rice cultivation in northeastern Heilongjiang Province from 2005 to 2010. In contrast, the area of rice cultivation in Liaoning Province remained relatively stable throughout the entire period from 1985 to 2023.

https://doi.org/10.5194/essd-2024-516
Preprint. Discussion started: 29 January 2025

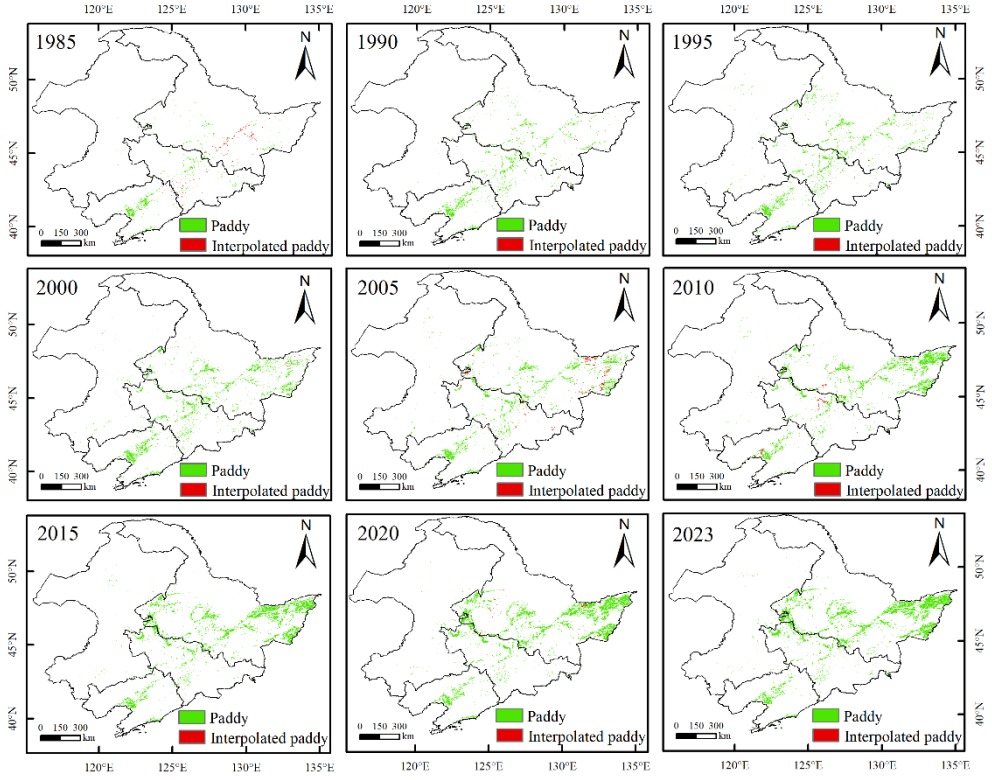

Figure 7: Spatial distribution of paddy rice in Northeast China.

We examined the changes in paddy field distribution in Northeast China from 1985 to 2023. The changes are illustrated in Fig.8. The paddy area in the study area exhibited significant growth, with a net increase of 5.34×10^4 km^2. Different provinces exhibited varying patterns of change. Heilongjiang province saw the largest increase in paddy area, with a gain of 4.33×10^4 km^2 from 1985 to 2023, followed by Jilin province with a 0.70×10^4 km^2 increase. Liaoning province and northeastern Inner Mongolia experienced smaller increases, with 0.16×10^4 km^2 and 0.15×10^4 km^2, respectively. This suggests that regions at high latitudes have become more suitable for paddy rice cultivation in recent decades. Additionally, Liaoning province experienced the largest reduction in paddy rice cultivation area, with a decrease of 0.20×10^4 km^2, followed by Jilin province, Heilongjiang province, and northeastern Inner Mongolia with a decrease of 0.09×10^4 km^2, 0.03×10^4 km^2 and 0.01×10^4 km^2, respectively.

https://doi.org/10.5194/essd-2024-516
Preprint. Discussion started: 29 January 2025

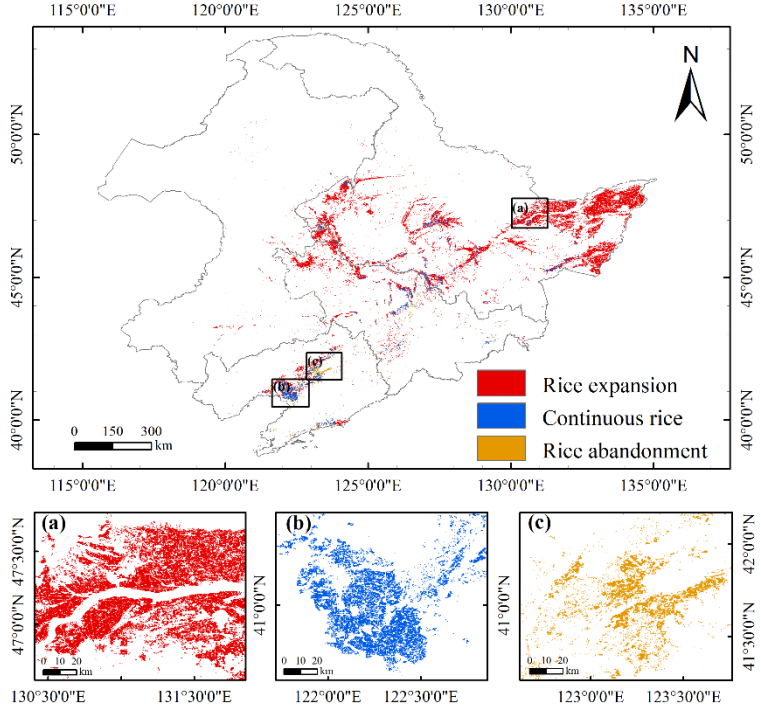

Figure 8: Trends of paddy rice cultivation area in Northeast China from 1985 to 2023.

4 Discussion

4.1 How the cross-sensor training sample impacts the accuracy of long history mapping

The Landsat 8/9 OLI sensor is an improvement and enhancement of the Landsat 5 TM sensor. It shares many characteristics such as the same spatial resolution, scene size, etc. However, there are slight differences in spectral range and sensor radiation calibration quality. These differences lead to variations in feature distribution, impacting the accuracy of crop mapping. This study focuses on the impact of these differences on paddy rice mapping accuracy. We conducted a comprehensive paddy rice mapping using an across-sensor training dataset to understand how these differences affect the accuracy of the model and how we can combine this dataset to achieve the best mapping accuracy. In this study, we employed nine different combinations of training and test sets to assess the performance of the cross-sensor dataset for paddy rice mapping in Northeast China (Table 4).

Table 4 Performance of different combinations of training and test datasets.

Combination Num.	Training set	Test set	F1	UA	PA
1	Landsat 5	Landsat 5	0.85	0.83	0.89
2	Landsat 5	Landsat 8	0.48	0.46	0.53
3	Landsat 8	Landsat 5	0.53	0.51	0.57
4	Landsat 8	Landsat 8	0.86	0.84	0.90
5	Landsat 5	Landsat 5+Landsat 8	0.62	0.61	0.65

https://doi.org/10.5194/essd-2024-516
Preprint. Discussion started: 29 January 2025

6	Landsat 8	Landsat 5+Landsat 8	0.64	0.62	0.67
7	Landsat 5+Landsat 8	Landsat 5+Landsat 8	0.84	0.82	0.88
8	Landsat 5 (Transfer learning with Landsat 8)	Landsat 8	0.67	0.65	0.70
9	Landsat 8 (Transfer learning with Landsat 5)	Landsat 5	0.70	0.68	0.74

In Table 4, we observed varying classification accuracy performances when using different combinations of training and test datasets. Combinations with minimal differences in feature distribution between the training and test datasets tended to have higher mapping accuracy. For example, combination numbers 1 and 4 achieved the highest values for the F1 score, UA, and PA. However, combination numbers 2 and 3, which had significant feature distribution differences between the training and test datasets, exhibited the lowest values of F1 score, UA, and PA. This suggests that when mapping paddy rice over a long history, using data from only one sensor may not yield reasonable results due to differences in feature distribution between sensors.

Furthermore, we implemented transfer learning by utilizing partial Landsat 5 TM or Landsat 8/9/ OLI data as the training set to fine-tune the models developed using combination numbers 1 and 4. Specifically, 20% of the Landsat 5 TM or Landsat 8/9 OLI images were selected as the training set to fine-tune the model originally trained with a training sample of combination numbers 1 and 4. The results revealed that fine-tuning the models enhanced accuracy. However, the accuracy of the fine-tuned models was lower than that of the models trained using a cross-sensor dataset, or the same sensor data, i.e. combination numbers 1, 4, and 7.

In summary, due to differences in spectral ranges, spectral characteristics, and spectral responses between the Landsat 5 TM and Landsat 8/9 OLI sensors, it is essential to use sufficient numbers of training data to achieve fine-mapping results. Moreover, while model fine-tuning can improve accuracy and generalization ability, it may not be effective for crop mapping in this case, especially when dealing with a long history and data from different sensors.

4.2 Contribution of ARE method in overcoming errors caused by feature differences in training and test dataset

Landsat images exhibit significant differences in spectral and spatial characteristics during the different growth periods of paddy rice. However, it is challenging to gather sufficient training samples to cover the entire growth period of paddy rice on a large scale and over an extended period. Consequently, the trained model may struggle to learn the features present in the test dataset on a large scale, leading to significant differences in the mapping results of paddy rice at different phenological stages. Figure 10 illustrates the difference in paddy rice results between the overlay and ARE methods. Compared to the ARE result, the overlay method exhibits a phenomenon of misclassification (Fig.9 (b)). As shown in Fig.9 (a) and (c), pixels with a lower category probability mean a significant difference between the learned features of FR-Net and the features of the predicted images. These uncertainties were inherited by the overlay method, but the ARE method selected the best category probability and thus presented fewer false alarms or omissions, as shown in Fig.9 (d).

https://doi.org/10.5194/essd-2024-516
Preprint. Discussion started: 29 January 2025

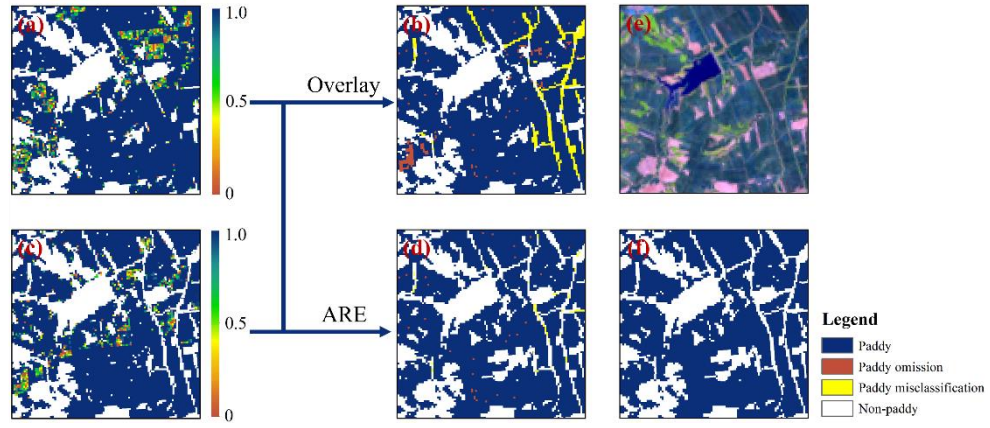

Figure 9: Comparison of paddy rice results between overlay and ARE results. (a) and (c) show the category possibilities for identifying paddy rice at different stages. (b) presents the overlay result, while (d) displays the ARE result. (e) depicts the pseudo-colored map, and (f) is the true map of paddy rice based on manual interpretation.

To assess the capability of ARE in overcoming the differences in features between training and test samples in different phenological periods and regions, we used the Landsat images with a Path/Row of 120/028 in 2016 as an example. We evaluated the UA, PA, and F1 scores of paddy rice mappings from individual phenological periods and the ARE paddy rice map (Table 5). In this work, we used the image acquired on May 31st as the training set, and the images from other periods were individually used as the test set to demonstrate the effectiveness of the ARE method in enhancing paddy rice mapping results at different phenological stages.

Table 5 Comparison of accuracy among single phenological period maps and the ARE paddy rice map.

Training image date	Testing image date	Matrices		
		UA	PA	F1
31/05	16 June 2016	0.66	0.95	0.74
	02 July 2016	0.62	0.87	0.72
	18 July 2016	0.59	0.80	0.68
	03 August 2016	0.58	0.77	0.67
	19 August 2016	0.63	0.92	0.71
	20 September 2016	0.52	0.66	0.64
ARE map		0.92	0.94	0.93

Moreover, we separately utilized Landsat images from different regions in the same year as the test set to evaluate the accuracy of the FR-Net model and then compared the accuracy of paddy rice maps from different regions within the same year with those achieved by the ARE method. The Landsat images with different Path/Row in 2016 were used as the inputs to calculate the UA, PA, and F1 scores of FR-Net (Table 6).

Table 6 Comparison of accuracy among the paddy rice maps with different Path/Row and the ARE paddy rice map.

Training image Path/Row	Testing image Path/Row	Matrices

https://doi.org/10.5194/essd-2024-516
Preprint. Discussion started: 29 January 2025

		UA	PA	F1 score
116/026	116/028	0.68	0.58	0.59
	120/026	0.32	0.44	0.37
	120/027	0.71	0.79	0.73
	120/028	0.70	0.64	0.65
	120/029	0.15	0.34	0.17
	122/030	0.06	0.21	0.09
ARE map		0.91	0.93	0.92

Tables 5 and 6 confirmed the benefits of using the ARE method to significantly improve the temporal and spatial mapping accuracy of FR-Net for paddy rice. Additionally, optimizing the mappings of paddy rice based on multiple phenological periods can help diminish the impact of cloud cover on satellite image quality. Therefore, introducing the ARE method is crucial for enhancing the accuracy of paddy rice maps in large-scale and long history mapping.

4.3 Uncertainties in paddy rice classification

As the results and comparison are shown in this study, the presented ARE method can effectively improve the annual mapping accuracy by using category probability at different phenological periods. However, it also has limitations. First, the ARE method improves mapping accuracy by processing multiple classification category probability of FR-Net and cannot improve mapping accuracy when only a single image is available. Furthermore, the efficacy of the ARE method is intricately linked to the quantity and quality of the training samples. When the quantity and quality of training samples are limited, the confidence of the category probability of the paddy rice mapping results integrated into the ARE method is low, the improvement in precision that the ARE method can provide may be insignificant. Finally, due to the time restrictions of field investigations and the availability of Google Earth data, this study only validated the paddy rice mapping results from 1985 to 2001 using agricultural statistical data, which may reduce the confidence level in the long history mapping. Therefore, continuous improvement of methods and techniques is essential to enhance the reliability of paddy rice mappings in light of the current issues associated with ARE methods.

5 Code/Data availability

The FR-Net codes are available at https://github.com/xialang2012/Paddy. The paddy rice maps produced with 30 m resolution in this study are accessible at https://doi.org/10.6084/m9.figshare.27604839.v1 (Zhang et al., 2024). The dataset includes a set of GeoTIFF images in the ESPG: 4326 spatial reference system. The values 1 and 0 represent paddy and non-paddy, respectively. We encourage users to independently verify the paddy rice maps. In addition, Landsat 5 TM and Landsat 8/9 OLI are available on United States Geological Survey (USGS) (https://earthexplorer.usgs.gov).

https://doi.org/10.5194/essd-2024-516
Preprint. Discussion started: 29 January 2025

6 Conclusions

This study developed a cross-sensor training dataset for recognizing paddy rice in Northeast China from 1985 to 2023 at a 30-meter spatial resolution. The presented annual result enhancement (ARE) method, which considers the differences in category probability of FR-Net at different growth stages to alleviate the impact of the limited training sample in large-scale and across-sensors paddy rice mapping. The ARE method showed a 6% increase in the F1 score than the compared methods, with UA, PA, F1 score, and MCC values of 0.92, 0.95, 0.93, and 0.81, respectively. Compared to other traditional classification methods, the results of this study demonstrate improved mapping accuracy, with a 4% increase in UA, 7% in PA, 6% in F1 score, and 14% in MCC. The overall trend from 1985 to 2023 indicated a significant increase of 5.34×10^4 km^2 in the rice cultivation area, expanded by 4.81 times. In all, this study confirmed that the semantic segmentation network FR-Net and ARE methods could accurately realize the large-scale and long-history monitoring of paddy rice, and it would provide a paddy rice classification dataset to detect the spatiotemporal patterns and dynamic mechanisms of paddy rice.

Author contributions

Z.Z., L.X., and F.Z. designed the study and the methodology, Z.Z. and L.X. wrote the code and generated the data, Y.G., J.Y., and Y.Z. provided the ground truth data, Z.Z., S.W., and P.Y. and checked samples and evaluate the resulting maps. All authors analyzed the data, wrote, and edited the manuscript.

Competing interests

The authors declare that they have no known competing financial interests or personal relationships that could have appeared to influence the work reported in this paper.

Acknowledgments

This work was supported by grants from the National Key Research and Development Program of China (Award No. 2022YFD2001105), the National Natural Science Foundation of China (Award No. 42401448), the open project of State Key Laboratory of Efficient Utilization of Arid and Semi-arid Arable Land in Northern China, the Institute of Agricultural Resources and Regional Planning, Chinese Academy of Agricultural Sciences (EUAL-2023-02), the Agricultural Science and Technology Innovation Project of the Chinese Academy of Agriculture Sciences.

References

Akkem, Y., Biswas, S. K., and Varanasi, A.: Smart farming using artificial intelligence: A review, Engineering Applications of Artificial Intelligence, 120, 105899, https://doi.org/10.1016/j.engappai.2023.105899, 2023.

https://doi.org/10.5194/essd-2024-516
Preprint. Discussion started: 29 January 2025

Ashourloo, D., Nematollahi, H., Huete, A., Aghighi, H., Azadbakht, M., Shahrabi, H. S., and Goodarzdashti, S.: A new phenology-based method for mapping wheat and barley using time-series of Sentinel-2 images, Remote Sensing of Environment, 280, 113206, https://doi.org/10.1016/j.rse.2022.113206, 2022.

Chen, Z., Xu, H., Jiang, P., Yu, S., Lin, G., Bychkov, I., Hmelnov, A., Ruzhnikov, G., Zhu, N., and Liu, Z.: A transfer Learning-Based LSTM strategy for imputing Large-Scale consecutive missing data and its application in a water quality prediction system, Journal of Hydrology, 602, 126573, https://doi.org/10.1016/j.jhydrol.2021.126573, 2021.

Deines, J. M., Kendall, A. D., Crowley, M. A., Rapp, J., Cardille, J. A., and Hyndman, D. W.: Mapping three decades of annual irrigation across the US High Plains Aquifer using Landsat and Google Earth Engine, Remote Sensing of Environment, 233, 111400, https://doi.org/10.1016/j.rse.2019.111400, 2019.

Dong, J., Xiao, X., Kou, W., Qin, Y., Zhang, G., Li, L., Jin, C., Zhou, Y., Wang, J., Biradar, C., Liu, J., and Moore, B.: Tracking the dynamics of paddy rice planting area in 1986–2010 through time series Landsat images and phenology-based algorithms, Remote Sensing of Environment, 160, 99–113, https://doi.org/10.1016/j.rse.2015.01.004, 2015.

FAO: World Food and Agriculture – Statistical Yearbook 2023, FAO, https://doi.org/10.4060/cc8166en, 2023.

Feng, F., Gao, M., Liu, R., Yao, S., and Yang, G.: A deep learning framework for crop mapping with reconstructed Sentinel-2 time series images, Computers and Electronics in Agriculture, 213, 108227, https://doi.org/10.1016/j.compag.2023.108227, 2023.

Foody, G. M.: Explaining the unsuitability of the kappa coefficient in the assessment and comparison of the accuracy of thematic maps obtained by image classification, Remote Sensing of Environment, 239, 111630, https://doi.org/10.1016/j.rse.2019.111630, 2020.

Gao, Y., Pan, Y., Zhu, X., Li, L., Ren, S., Zhao, C., and Zheng, X.: FARM: A fully automated rice mapping framework combining Sentinel-1 SAR and Sentinel-2 multi-temporal imagery, Computers and Electronics in Agriculture, 213, 108262, https://doi.org/10.1016/j.compag.2023.108262, 2023.

Goldberg, K., Herrmann, I., Hochberg, U., and Rozenstein, O.: Generating Up-to-Date Crop Maps Optimized for Sentinel-2 Imagery in Israel, Remote Sensing, 13, 3488, https://doi.org/10.3390/rs13173488, 2021.

Graesser, J. and Ramankutty, N.: Detection of cropland field parcels from Landsat imagery, Remote Sensing of Environment, 201, 165–180, https://doi.org/10.1016/j.rse.2017.08.027, 2017.

Griffiths, P., Nendel, C., and Hostert, P.: Intra-annual reflectance composites from Sentinel-2 and Landsat for national-scale crop and land cover mapping, Remote Sensing of Environment, 220, 135–151, https://doi.org/10.1016/j.rse.2018.10.031, 2019.

Griffiths, P., Nendel, C., Pickert, J., and Hostert, P.: Towards national-scale characterization of grassland use intensity from integrated Sentinel-2 and Landsat time series, Remote Sensing of Environment, 238, 111124, https://doi.org/10.1016/j.rse.2019.03.017, 2020.

Guo, Y. and Ren, H.: Remote sensing monitoring of maize and paddy rice planting area using GF-6 WFV red edge features, Computers and Electronics in Agriculture, 207, 107714, https://doi.org/10.1016/j.compag.2023.107714, 2023.

Huang, Y., Qiu, B., Chen, C., Zhu, X., Wu, W., Jiang, F., Lin, D., and Peng, Y.: Automated soybean mapping based on canopy water content and chlorophyll content using Sentinel-2 images, International Journal of Applied Earth Observation and Geoinformation, 109, 102801, https://doi.org/10.1016/j.jag.2022.102801, 2022.

Jin, T. and Zhong, T.: Changing rice cropping patterns and their impact on food security in southern China, Food Sec., 14, 907–917, https://doi.org/10.1007/s12571-022-01254-3, 2022.

Kamir, E., Waldner, F., and Hochman, Z.: Estimating wheat yields in Australia using climate records, satellite image time series and machine learning methods, ISPRS Journal of Photogrammetry and Remote Sensing, 160, 124–135, https://doi.org/10.1016/j.isprsjprs.2019.11.008, 2020.

Khojastehnazhand, M. and Roostaei, M.: Classification of seven Iranian wheat varieties using texture features, Expert Systems with Applications, 199, 117014, https://doi.org/10.1016/j.eswa.2022.117014, 2022.

Kong, W., Dong, Z. Y., Jia, Y., Hill, D. J., Xu, Y., and Zhang, Y.: Short-Term Residential Load Forecasting Based on LSTM Recurrent Neural Network, IEEE Trans. Smart Grid, 10, 841–851, https://doi.org/10.1109/TSG.2017.2753802, 2019.

Liang, S., Wu, W., Sun, J., Li, Z., Sun, X., Chen, H., Chen, S., Fan, L., You, L., and Yang, P.: Climate-mediated dynamics of the northern limit of paddy rice in China, Environ. Res. Lett., 16, 064008, https://doi.org/10.1088/1748-9326/abfac0, 2021.

Liu, W., Dong, J., Xiang, K., Wang, S., Han, W., and Yuan, W.: A sub-pixel method for estimating planting fraction of paddy rice in Northeast China, Remote Sensing of Environment, 205, 305–314, https://doi.org/10.1016/j.rse.2017.12.001, 2018.

Lu, T., Gao, M., and Wang, L.: Crop classification in high-resolution remote sensing images based on multi-scale feature fusion semantic segmentation model, Front. Plant Sci., 14, 1196634, https://doi.org/10.3389/fpls.2023.1196634, 2023.

Luo, Y., Zhang, Z., Chen, Y., Li, Z., and Tao, F.: ChinaCropPhen1km: a high-resolution crop phenological dataset for three staple crops in China during 2000–2015 based on leaf area index (LAI) products, Earth Syst. Sci. Data, 12, 197–214, https://doi.org/10.5194/essd-12-197-2020, 2020.

Ni, R., Tian, J., Li, X., Yin, D., Li, J., Gong, H., Zhang, J., Zhu, L., and Wu, D.: An enhanced pixel-based phenological feature for accurate paddy rice mapping with Sentinel-2 imagery in Google Earth Engine, ISPRS Journal of Photogrammetry and Remote Sensing, 178, 282–296, https://doi.org/10.1016/j.isprsjprs.2021.06.018, 2021.

Onojeghuo, A. O., Blackburn, G. A., Wang, Q., Atkinson, P. M., Kindred, D., and Miao, Y.: Mapping paddy rice fields by applying machine learning algorithms to multi-temporal Sentinel-1A and Landsat data, International Journal of Remote Sensing, 39, 1042–1067, https://doi.org/10.1080/01431161.2017.1395969, 2018.

Pan, L., Xia, H., Zhao, X., Guo, Y., and Qin, Y.: Mapping Winter Crops Using a Phenology Algorithm, Time-Series Sentinel-2 and Landsat-7/8 Images, and Google Earth Engine, Remote Sensing, 13, 2510, https://doi.org/10.3390/rs13132510, 2021.

Shao, Q., Li, R., Qiu, J., Han, Y., Han, D., Chen, M., and Chi, H.: Large-scale mapping of new mixed rice cropping patterns in southern China with phenology-based algorithm and MODIS dataset, Paddy Water Environ, 21, 243–261, https://doi.org/10.1007/s10333-023-00926-w, 2023.

Shen, R., Pan, B., Peng, Q., Dong, J., Chen, X., Zhang, X., Ye, T., Huang, J., and Yuan, W.: High-resolution distribution maps of single-season rice in China from 2017 to 2022, Earth Syst. Sci. Data, 15, 3203–3222, https://doi.org/10.5194/essd-15-3203-2023, 2023.

Shi, D., Huang, Q., Liu, Z., Liu, T., Su, Z., Guo, S., Bai, F., Sun, S., Lin, X., Li, T., and Yang, X.: Radiation use efficiency and biomass production of maize under optimal growth conditions in Northeast China, Science of The Total Environment, 836, 155574, https://doi.org/10.1016/j.scitotenv.2022.155574, 2022.

Sun, C., Zhang, H., Xu, L., Ge, J., Jiang, J., Zuo, L., and Wang, C.: Twenty-meter annual paddy rice area map for mainland Southeast Asia using Sentinel-1 synthetic-aperture-radar data, Earth Syst. Sci. Data, 15, 1501–1520, https://doi.org/10.5194/essd-15-1501-2023, 2023.

Sun, L., Gao, F., Xie, D., Anderson, M., Chen, R., Yang, Y., Yang, Y., and Chen, Z.: Reconstructing daily 30 m NDVI over complex agricultural landscapes using a crop reference curve approach, Remote Sensing of Environment, 253, 112156, https://doi.org/10.1016/j.rse.2020.112156, 2021.

Thorp, K. R. and Drajat, D.: Deep machine learning with Sentinel satellite data to map paddy rice production stages across West Java, Indonesia, Remote Sensing of Environment, 265, 112679, https://doi.org/10.1016/j.rse.2021.112679, 2021.

Xia, L., Zhao, F., Chen, J., Yu, L., Lu, M., Yu, Q., Liang, S., Fan, L., Sun, X., Wu, S., Wu, W., and Yang, P.: A full resolution deep learning network for paddy rice mapping using Landsat data, ISPRS Journal of Photogrammetry and Remote Sensing, 194, 91–107, https://doi.org/10.1016/j.isprsjprs.2022.10.005, 2022.

Xiao, X., Boles, S., Liu, J., Zhuang, D., Frolking, S., Li, C., Salas, W., and Moore, B.: Mapping paddy rice agriculture in southern China using multi-temporal MODIS images, Remote Sensing of Environment, 95, 480–492, https://doi.org/10.1016/j.rse.2004.12.009, 2005.

Xin, F., Xiao, X., Dong, J., Zhang, G., Zhang, Y., Wu, X., Li, X., Zou, Z., Ma, J., Du, G., Doughty, R. B., Zhao, B., and Li, B.: Large increases of paddy rice area, gross primary production, and grain production in Northeast China during 2000–2017, Science of The Total Environment, 711, 135183, https://doi.org/10.1016/j.scitotenv.2019.135183, 2020.

Xu, S., Zhu, X., Chen, J., Zhu, X., Duan, M., Qiu, B., Wan, L., Tan, X., Xu, Y. N., and Cao, R.: A robust index to extract paddy fields in cloudy regions from SAR time series, Remote Sensing of Environment, 285, 113374, https://doi.org/10.1016/j.rse.2022.113374, 2023.

Xuan, F., Dong, Y., Li, J., Li, X., Su, W., Huang, X., Huang, J., Xie, Z., Li, Z., Liu, H., Tao, W., Wen, Y., and Zhang, Y.: Mapping crop type in Northeast China during 2013–2021 using automatic sampling and tile-based image classification, International Journal of Applied Earth Observation and Geoinformation, 117, 103178, https://doi.org/10.1016/j.jag.2022.103178, 2023.

Yang, J., Hu, Q., Li, W., Song, Q., Cai, Z., Zhang, X., Wei, H., and Wu, W.: An automated sample generation method by integrating phenology domain optical-SAR features in rice cropping pattern mapping, Remote Sensing of Environment, 314, 114387, https://doi.org/10.1016/j.rse.2024.114387, 2024.

Yang, L., Huang, R., Huang, J., Lin, T., Wang, L., Mijiti, R., Wei, P., Tang, C., Shao, J., Li, Q., and Du, X.: Semantic Segmentation Based on Temporal Features: Learning of Temporal–Spatial Information From Time-Series SAR Images for Paddy Rice Mapping, IEEE Trans. Geosci. Remote Sensing, 60, 1–16, https://doi.org/10.1109/TGRS.2021.3099522, 2022.

Yeom, J.-M., Jeong, S., Deo, R. C., and Ko, J.: Mapping rice area and yield in northeastern asia by incorporating a crop model with dense vegetation index profiles from a geostationary satellite, GIScience & Remote Sensing, 58, 1–27, https://doi.org/10.1080/15481603.2020.1853352, 2021.

Yin, L., You, N., Zhang, G., Huang, J., and Dong, J.: Optimizing Feature Selection of Individual Crop Types for Improved Crop Mapping, Remote Sensing, 12, 162, https://doi.org/10.3390/rs12010162, 2020.

You, N., Dong, J., Huang, J., Du, G., Zhang, G., He, Y., Yang, T., Di, Y., and Xiao, X.: The 10-m crop type maps in Northeast China during 2017–2019, Sci Data, 8, 41, https://doi.org/10.1038/s41597-021-00827-9, 2021.

https://doi.org/10.5194/essd-2024-516
Preprint. Discussion started: 29 January 2025

Zhang, C., Zhang, H., and Tian, S.: Phenology-assisted supervised paddy rice mapping with the Landsat imagery on Google Earth Engine: Experiments in Heilongjiang Province of China from 1990 to 2020, Computers and Electronics in Agriculture, 212, 108105, https://doi.org/10.1016/j.compag.2023.108105, 2023.

Zhang, J., Feng, L., and Yao, F.: Improved maize cultivated area estimation over a large scale combining MODIS–EVI time series data and crop phenological information, ISPRS Journal of Photogrammetry and Remote Sensing, 94, 102–113, https://doi.org/10.1016/j.isprsjprs.2014.04.023, 2014.

Zhang, Z.: **Long history paddy rice mapping across Northeast China with deep learning and annual result enhancement method-Training Dataset**, https://doi.org/10.6084/M9.FIGSHARE.28283606, 2025.

Zhang, Z., Xia, L., Zhao, F., Gu, Y., Yang, J., Zha, Y., Wu, S., and Yang, P.: Long history paddy rice mapping across Northeast China with deep learning and annual result enhancement method, https://doi.org/10.6084/M9.FIGSHARE.27604839.V1, 2024.

Zheng, B., Wang, J., Wu, S., Wu, H., Xie, Z., and Wan, W.: Spatio-temporal patterns and driving mechanisms of rice biomass during the growth period in China since 2000, Ecological Indicators, 153, 110389, https://doi.org/10.1016/j.ecolind.2023.110389, 2023.

Zhong, L., Hu, L., and Zhou, H.: Deep learning based multi-temporal crop classification, Remote Sensing of Environment, 221, 430–443, https://doi.org/10.1016/j.rse.2018.11.032, 2019.

Zhu, Q.: On the performance of Matthews correlation coefficient (MCC) for imbalanced dataset, Pattern Recognition Letters, 136, 71–80, https://doi.org/10.1016/j.patrec.2020.03.030, 2020.